Sixth International Conference on Durability of Concrete Structures **Paper Number PSE18**
18 - 20 July 2018
University of Leeds, Leeds, West Yorkshire, LS2 9JT, United Kingdom

Electrochemical Behaviour of Passive Layers in Weathered Reinforced Mortars

B. Díaz, B. Guitián, X.R. Nóvoa and M.C. Pérez
University of Vigo, Campus Universitario, Vigo, Spain

ABSTRACT

Electrochemical methods are widely employed for assessing the corrosion performance of steel rebars embedded in concrete. Corrosion potential and polarization resistance are the main parameters considered for this purpose; under the assumption that the cathodic process corresponds to oxygen reduction and the anodic process to steel corrosion. Although these assumptions are mostly true, they are not able to explain some transitions from passive to active states, as well as some corrosion potential evolutions. The present contribution is intended to provide an in depth approximation to those questions based on the study of thick passive layers formed over years in atmospheric exposure. Results for blank samples and samples containing chlorides are discussed based on findings from electrochemical impedance spectroscopy. Temperature was considered in the study as a parameter for acting on both the chemistry of the pore electrolyte and the specific volume of the oxides layer. By this approach, we were able to identify the contribution of the oxides layer to the impedance spectra in the 10 kHz-1 Hz frequency range. The oxides layer supports the oxygen cathodic reaction, but also the anodic and cathodic processes corresponding to the re-oxidation and reduction of the layer itself. Compared to layers formed in the absence of chlorides, the presence of chlorides in the concrete mix leads to the formation of a more oxidised oxide layer, with decreased redox activity and more prone to cracking under thermal cycling.

Keywords: Passivity of steel in concrete; long time exposure; temperature effect; porous electrode; electrochemical impedance.

1.0 INTRODUCTION

Formation of the passivation layer and its chemical and mechanical stability are key factors for the durability of the reinforced concrete structures. There is consensus on the fact that passive layers degrade mainly due to carbonation of concrete and/or the presence of chlorides. Consideration of these two aspects is necessary for reliable lifetime predictions. However, exposure conditions regarding wetting and drying cycles and temperature fluctuations are also relevant environmental factors not usually taken into account.

Multiple studies have addressed the formation and stability of the passive film in solutions simulating the concrete pore environment (Flis 1996; Joiret *et al.* 2002; Moreno *et al.* 2004; Sánchez *et al.* 2007; Ghods *et al.* 2009; Freire *et al.* 2012). However, few studies deal with the long-term behaviour, over which reinforced concrete specimens must be considered (Vidal, Castel, and François 2007; Bautista *et al.* 2015; Serdar, Žulj, and Bjegović 2013). A limited number of studies have included temperature as a factor influencing the corrosion performance. Some simulation models (Pour-Ghaz, Isgor, and Ghods 2009) show an increased corrosion rate with discrete increases in the temperature, although no changes in the passive layer were reported. Similar results were derived from studies on the effect of seasonal and daily temperature cycles (Andrade, Alonso, and Sarría 2002). Modifications in the passive layer composition with temperature increase have been reported, particularly an increased oxidation level and hydration degree (Deus *et al.* 2012), thus demonstrating the influence of temperature on passive film protectiveness. Temperature changes also affect the chemistry of the pore solution, which in turn affects the developed passive layers.

Here we describe the influence of the presence of chlorides in the mortar mix on the electrochemical behaviour of embedded steel rebars after 15 years of exposure to the atmosphere. Temperature cycles and electrochemical impedance spectroscopy (EIS) were employed as sensing techniques. The EIS data were modelled using a modification of the transmission line model originally developed by Macdonald (Park and Macdonald 1983) for the study of porous conducting layers(Guitián *et al.* 2013; Díaz *et al.* 2015; Díaz *et al.* 2018).

2.0 EXPERIMENTAL

The test specimens were prepared as described elsewhere (Andrade, Merino, *et al.* 1995) using

cement CEM I 52.5R, w/c = 0.5, s/c = 3. The sand was ϕ < 6 mm. The chloride containing specimens were prepared by adding to the water mix 2% $CaCl_2$ (relative to the cement weight). The rebars' diameter was 8 mm and an active surface of 13 cm^2 was delimited with elastic tape. The mortar cover was 2.7 cm. The specimens were cured for 28 days and then exposed for 15 years in a mild rural-marine atmosphere. This atmosphere is of class S1 and P0 in terms of chloride and SOx depositions, respectively, according to the ISO 9223:2012. The time of wetness in the test site is high (classified as T5). The ambient temperature ranges from 5 to 15 °C during wintertime and 15 to 30 °C in the summertime.

The electrochemical measurements, corrosion potential, E_{corr}, determination, and EIS were taken using a Metrohm- Autolab® PGSTat 30 device. The cell arrangement was that described elsewhere (Andrade, Soler, *et al.* 1995) for proper electric field distribution: A cylindrical mortar sample with the rebar placed at its revolution axis. The working electrode (WE) was the rebar studied, the counter electrode (CE) was a flexible graphite sheet surrounding the mortar cylinder, and the reference electrode (RE) was a saturated calomel electrode (SCE) placed on top of the arrangement. The ionic contact between the RE and CE with the mortar was assured with wet pads.

For temperature control, the specimens were partially immersed in a deionised water bath whose temperature was varied at 5 °C steps using a Lauda® Brinkman Ecoline Recirculating Chiller RE 415 thermostat. The electrochemical measurements were taken after a minimum of 24 h to ensure thermal equilibration at the rebar level (Nóvoa *et al.* 2016).

The surface and cross section of the rebars were examined by optical and electronic microscopies. For optical microscopy, an Olympus GX71/GX51 Inverted Metallurgical Microscope was employed. For the scanning electron microscopy (SEM) observation and energy dispersive X-ray (EDX) analyses, an Electroscan JSM-54 model JEOL 5410 equipped with an energy dispersive X-ray detector Link ISIS 300 was used.

3.0 RESULTS AND DISCUSSION

3.1 Characterisation of the oxide layer

The visual aspect of the rebars was that of uncorroded steel, with only a little rust-like colour. However, the cross-section view presented in Fig. 1 reveals the presence of an apparently homogeneous oxides layer of about 28 μm thick (Fig. 1A) with some cracks (Fig. 1B). Considering magnetite (density 36.4% lower than that of iron) or hematite (density 34% lower than that of iron) as the main corrosion products, the 28 μm of oxide thickness corresponds to about 18 μm of rebar thickness loss. i.e., an average of 1.2 μm/y, or 0.1 μA/cm^2 (considering the Fe/Fe^{2+} process). The range 0.1–0.2 μA/cm^2 is commonly considered as the threshold value between passivity and active corrosion (Alonso *et al.* 2000). Thus, the observed oxide scale corresponds well to a situation of passivity, as expected for the mild atmospheric conditions of exposure, although approaching the limit usually considered for active corrosion.

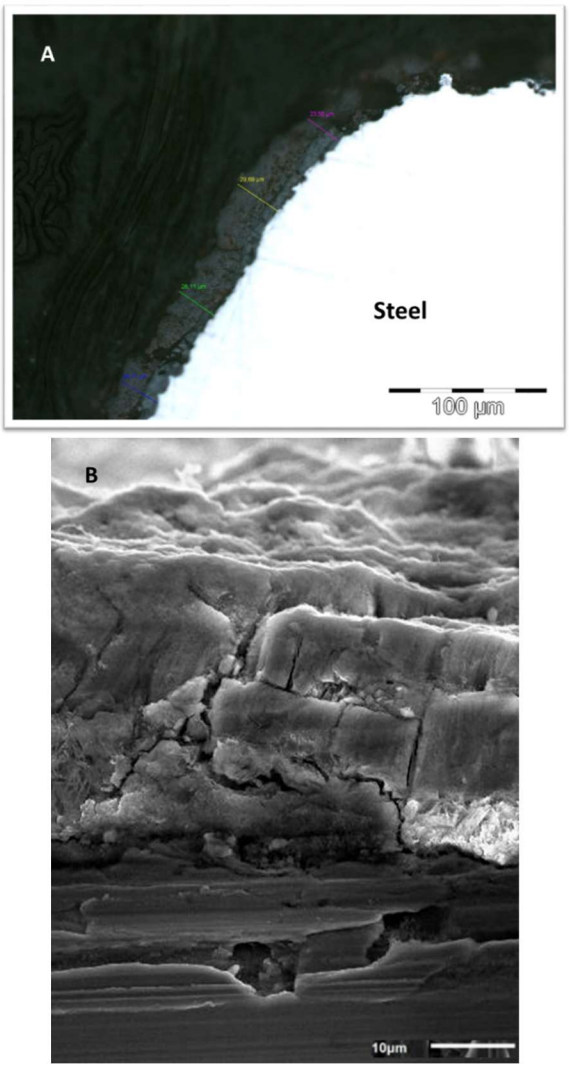

Fig. 1. A) Optical image and B) SEM image of the cross section of one of the rebars showing the morphology of the oxide layer, the thickness of which was estimated as 28 μm. Images corresponding to the reference sample

Because Ca was detected at the metal-oxide interface by EDX mapping (result not shown here), the cracks present in the oxides layer likely allow the electrolyte to access the metal-oxide interface. This finding is relevant for the corrosion behaviour, which we discuss below.

3.2 Temperature cycling

Figure 2 corresponds to the evolution of the corrosion potential with temperature during a thermal cycle starting at 5 °C. The data, plotted on the same ordinate scale for easy comparison, show a

difference of about 200 mV between the two conditions, with the sample containing chlorides being more active. Moreover, the thermal cycle seems to be reversible (in the time scale of the experiment) for the reference sample (Fig. 2A), while an important hysteresis is observed for the sample containing chlorides (Fig. 2B).

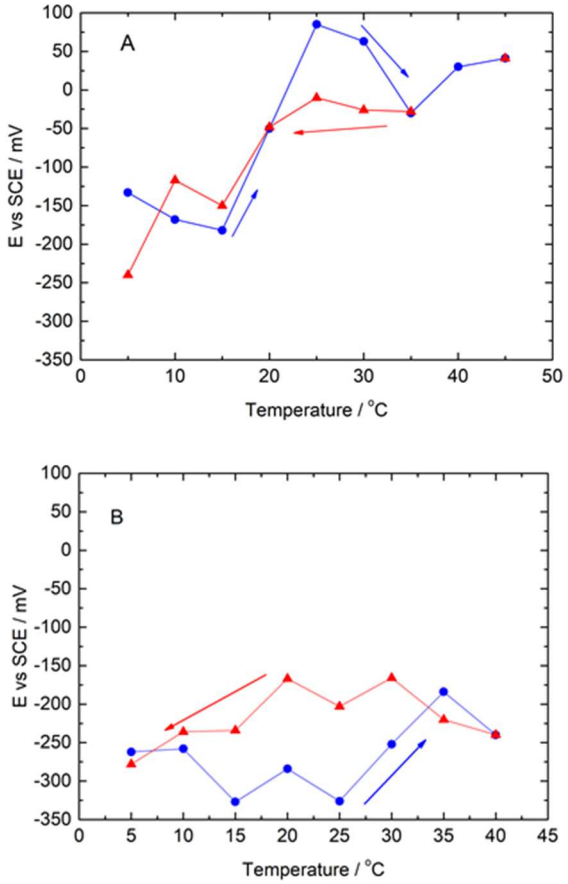

Fig. 2. Evolution of the corrosion potential with temperature in a thermal cycle starting at 5 °C: A) Reference sample; B) Sample with chlorides

The data presented in Fig. 2 allow the extraction of some preliminary information on the nature of both corrosion products. The higher potential values observed for Fig. 2A inform about the relative more importance of the participation of the oxides layer in the cathodic reaction for the sample without chlorides (Alonso *et al.* 1998). The hysteresis observed in Fig. 2B can be related to the presence of chlorides, which favours an irreversible reaction path via hydroxychlorides (Andrade *et al.* 2001).

3.3 EIS results and modelling

Figures 3 and 4 summarise the impedance spectra obtained for the reference sample and for that containing chlorides, respectively. The low-frequency region (~1 Hz to 1 mHz) is seen in Fig. 3A and Fig. 4A. The high-frequency region (100 kHz to ~10 Hz) corresponds to Fig. 3B and Fig. 4B. The low frequency spectra show a rough impedance decrease as temperature rises and, as expected, the impedance values are lower for the specimens containing chlorides. Extrapolation of the low-frequency arcs to the real axis provides polarization resistances (Rp) near or higher (depending on temperature) than 250 kΩ cm^2, i.e., corrosion current densities near 0.1 μA/cm^2 or lower, if B is taken as 26 mV in Eq. 1. This result is in good agreement with the thickness of the corrosion products layer presented in Fig. 1.

$$i_{corr} = B/R_p \qquad [1]$$

The most remarkable feature, however, appears in the high-frequency range, where up to three time constants can be distinguished. The diameters of this capacitive features decrease as temperature increases, and are smaller for the sample containing chlorides, which points to some effect of the pore electrolyte conductivity.

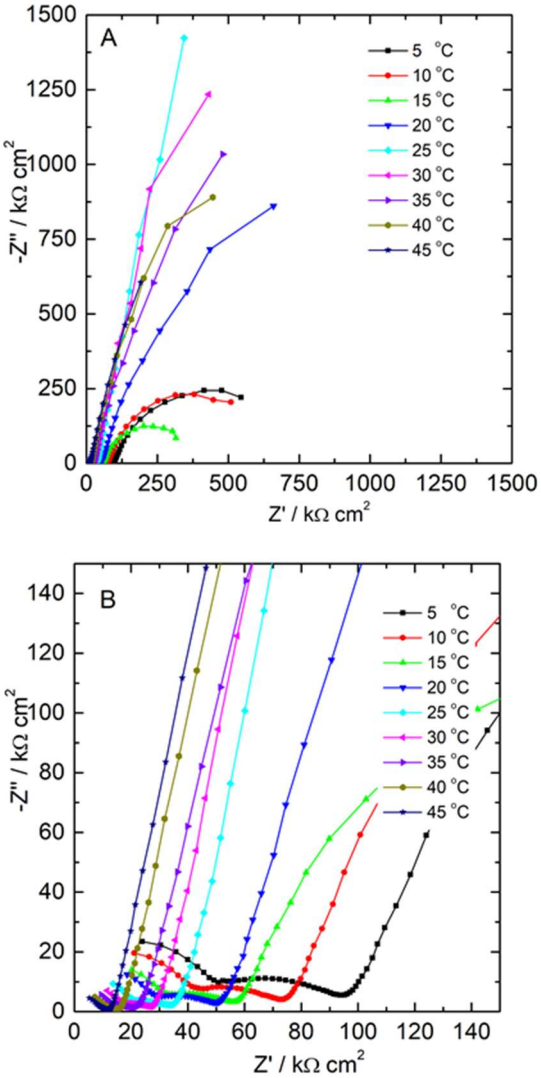

Fig. 3. Evolution of the impedance spectra with temperature for the sample without chlorides. A) Full spectrum down to 1 mHz. B) Detail of the high-frequency region.

The capacitive arc appearing in the high-frequency limit is more evident at low temperatures (see Fig. 3B) and shows characteristic frequencies at about

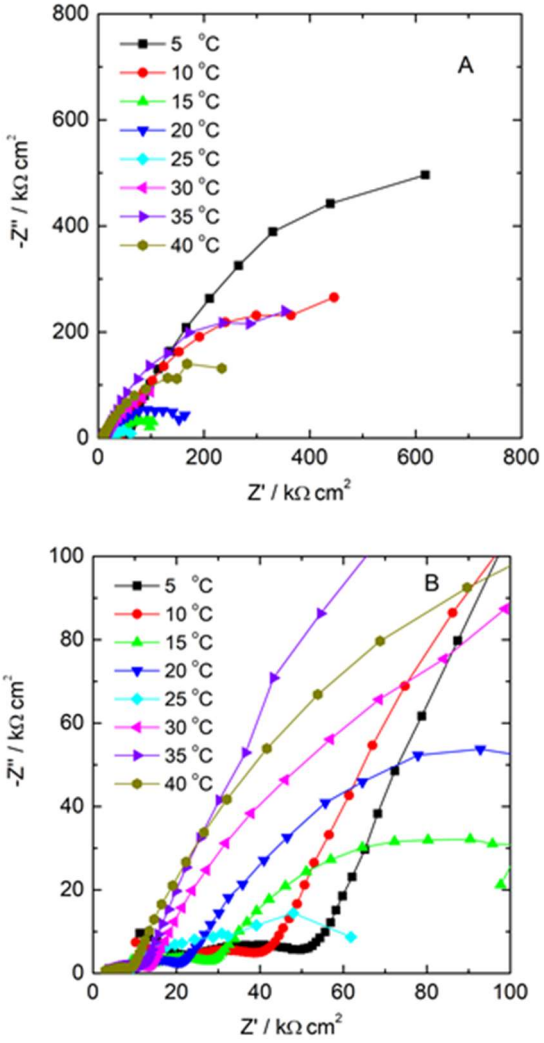

Fig. 4. Evolution of the impedance spectra with temperature for the sample with chlorides. A) Full spectrum down to 1 mHz. B) Detail of the high frequency region.

100 kHz or above. From this characteristic frequency and the associated parallel resistance estimated from the diameter of the corresponding capacitive arc, capacitances in the range of tenths of pF/cm^2 can be estimated, which allows to the association of this time constant to the dielectric contribution of the concrete cover.

According to the reasoning above, the high-frequency part of the impedance spectrum corresponds to the dielectric cover, while the low frequency part (f < ~ 1 Hz) corresponds to the anodic process linked to the corrosion rate. The central part of the spectrum, between ~10 kHz and ~10 Hz, remains unassigned, although it has to do in some way with the pore electrolyte resistivity because the diameter of the corresponding capacitive arc scales with temperature (Fig. 3B and 4B). Moreover, the conducting and redox character of iron corrosion products are widely recognised (Andrade *et al.* 2001; Sánchez-Moreno *et al.* 2009), with the oxides layer based on magnetite (Joiret *et al.* 2002). In this context, an electrical equivalent model can be set up considering a porous (see Fig. 1B) conducting structure where electronic conduction takes place through the solid phase, while ionic conduction (a parallel conducting path) occurs at pores filled with the electrolyte. The cathodic reaction will occur mainly at pore walls, overlapping a Fe^{3+}/Fe^{2+} transformation, while the genuine corrosion process will occur at the pore bottom.

Bringing all this together, the electrical equivalent depicted in Fig. 5 can be postulated to describe the recorded EIS spectra. Rs accounts for the pore electrolyte resistivity and Rm for the solid phase resistivity. The Z_i elements correspond to the impedance defined in Eq. 2, where $j=\sqrt{-1}$, $\omega = 2\pi f$ and α_i is the Cole-Cole dispersion coefficient of the R_iC_i time constant. Z_0 accounts for the impedance of the mortar cover, which is in series with the redox electrochemical system represented by the porous oxides (or hydroxichlorides) layer. Z_1 represents the reaction at pore walls that involves oxygen reduction and Fe^{3+}/Fe^{2+} transformation thus involving two RC time constants hierarchically distributed RC time constants, R_1C_1, and $R_{11}C_{11}$, respectively.

$$Z_i = \frac{R_i}{1+(j\omega R_i C_i)^{\alpha_i}} \qquad [2]$$

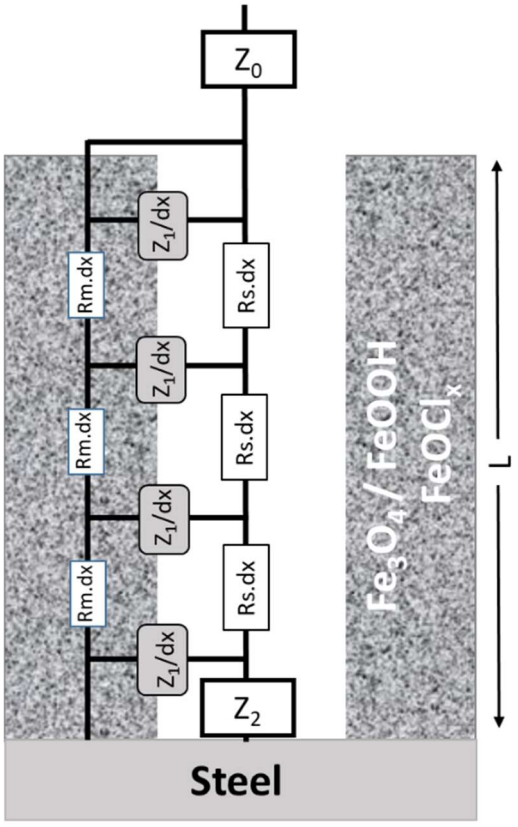

Fig. 5. Electrical equivalent representing the different physical phenomena that conform the recorded EIS spectra obtained for reinforced mortar samples.

The electrical equivalent depicted in Fig. 5 can reproduce the experimental impedance spectra, as

shown in Fig. 6, in the whole scanned frequency range, which validates the proposed electrical equivalent.

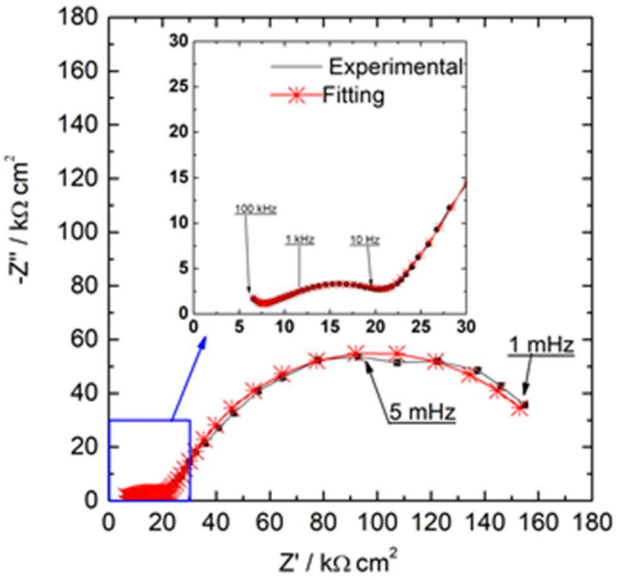

Fig. 6. Experimental and fitted EIS data obtained for the sample with chlorides, at 20 °C, during the forward temperature scan.

Table 1. Dependence of relevant parameters of the model on temperature rising (forward scan). Parameters for dielectric properties of the mortar cover (R_0C_0) and resistivity of the oxides layer, electronic resistivity (Rm) and ionic resistivity (Rs). The upper section corresponds to the reference sample, the lower section corresponds to the sample with chlorides.

Temp. (^{0}C)	R_0, (kΩ cm^2)	C_0 (pF/cm^2)	Rm (Ω cm)	Rs (MΩ cm)
5	36.9	48.6	7.4	24.2
10	30.6	54.7	3.8	21.1
15	22.0	57.1	9.5	17.7
20	19.9	60.0	1.0	16.0
25	15.0	81.8	6.5	10.2
30	12.4	84.5	21.8	8.0
35	10.1	99.9	22.3	6.9
40	10.3	110.0	12.3	3.1
45	8.8	140.0	24.0	2.0
5	25.4	80.8	83.6	10.0
10	14.9	88.2	1.7	10.0
15	8.0	61.9	79.4	9.9
20	4.9	77.3	25.6	8.9
25	2.2	100.0	13.9	3.0
30	2.7	100.0	10.8	4.1
35	2.8	69.3	10.6	4.8
40	2.1	99.7	21.5	3.5

The parameter values obtained from the fittings allow discussion of the evolution of the steel-concrete system under temperature cycling. Table 1 summarises the first set of values dealing with the conducting properties of the cover and the oxides layer.

Table 1 shows, as expected, a decreasing bulk mortar resistance with increasing temperature, although the temperature dependence is higher for the sample containing chloride. Moreover, the bulk capacitance increases with temperature, which can be related to portlandite precipitation and, consequently, increased pore surface. This variation is less remarkable for the sample containing chloride.

The resistivity of the solution in the pores of the oxides layer follows the same trend with temperature as in the bulk mortar. The absolute values inform about the percolating porosity of the layer. Regarding the resistivity of the solid phase, the trend is to increase with temperature for the reference sample. This fact relates to the progressive oxidation of the oxides layer as temperature increases. The dependence of the oxidation degree on temperature has been reported elsewhere (Deus *et al.* 2012). However, the presence of chlorides seems to hinder this process, as already derived from Fig. 2.

The parameters informing about the redox activity in the oxides layer are summarised in Table 2.

Table 2. Dependence of relevant parameters of the model on temperature rising (forward scan). Parameters for the cathodic reaction at pore walls (R_1C_1) and redox activity of the iron oxide ($R_{11}C_{11}$). The upper section corresponds to the reference sample, and the lower section corresponds to the sample with chlorides.

Temp. (^{0}C)	R_1, (Ω cm^3)	C_1 (μF/cm^3)	α_1	R_{11} (kΩ cm^3)	C_{11} (mF/ cm^3)	α_{11}
5	234.9	20.3	0.59	4.5	2.0	0.62
10	134.8	21.9	0.55	2.6	10	0.68
15	108.9	30.7	0.49	1.1	10	0.73
20	95.1	30.0	0.51	21.5	9.8	0.83
25	59.8	38.0	0.50	112.48	10	0.85
30	38.7	31.7	0.55	678.17	10	0.89
35	26.2	36.3	0.55	20.0	10	0.89
40	10.3	52.9	0.73	23.2	10	0.86
45	6.7	39.2	0.72	32.9	10	0.87
5	321.2	423.9	0.71	23.9	9.7	0.98
10	263.7	445.6	0.62	4.5	10	1.00
15	121.4	878.5	0.47	0.2	9.2	0.85
20	53.7	605.8	0.57	0.5	10	0.86
25	63.0	508.0	0.41	0.1	0.5	0.58
30	21.0	436.0	0.59	3.1	9.7	0.50
35	32.8	501.1	0.57	4.7	10	0.87
40	24.6	425.1	0.58	2.4	10	0.85

The parameter R_1 corresponds to the charge transfer resistance at pore walls (mainly due to oxygen

reduction because of accessibility). The values reported in Table 2 show that this process accelerates as temperature increases, following the Arrhenius equation. The activation energy for the sample without chlorides was estimated as 90.7 kJ/mol, whereas this value was just 40.6 kJ/mol for the sample containing chlorides, which corresponds to a faster oxygen reduction kinetics and is in agreement with the reported easier oxidability of the oxide layer in the presence of chlorides. The values of the dispersion coefficient α_1, which is close to 0.5, also suggests a mass transport controlled process.

The interfacial capacitances (C_1) are almost one order of magnitude higher for the sample containing chlorides, which suggests a more defective coating. Moreover, C_1 tends to increase with temperature for the sample without chlorides, which is likely related to crack formation that increases the active surface.

The dependence of the $R_{11}C_{11}$ time constant with temperature is not evident, although a limited increase with temperature can be observed for the sample without chlorides. This trend is in accordance with the evolution of the corrosion potential depicted in Fig. 2. The layer becomes oxidised as the temperature increases.

The kinetics of the corrosion process is, according to the model, represented by the R_2C_2 time constant, whose parameter values as a function of temperature are given in Table 3. It is interesting to see in this table that R_2 increases with temperature for the sample without chlorides, which means that the corrosion rate slows down, probably due to the formation of an oxidised adherent corrosion product layer. This kind of passivation process with temperature is not observed for the chloride-containing sample, for which R_2 remains almost independent of the temperature. R_2 values are higher for the sample without chlorides, which means a lower corrosion rate, especially for high temperatures.

Another interesting feature to highlight in Table 3 is the C_2 smooth trend to increase with temperature, for the sample without chlorides, which can be associated to an increased active surface due to crack formation associated with the Fe^{2+}/Fe^{3+} oxidation process. This variation is non-regular in the presence of chlorides. C_2 values oscillate during the temperature scan, which indicates a non-uniform evolution of the layer structure under thermal stress.

The effect of the thermal cycle on the reinforced mortar systems studied can be assessed visually using Figs. 7 and 8. The diameter of the high-frequency region decreases by 50% after the thermal cycle (Fig. 7A), which means that both the mortar cover and the oxides layer present higher density of ionic paths towards the metallic interface. Consequently, the low frequency limit of the

Table 3. Dependence of relevant parameters of the model on temperature rising (forward scan). Parameters for the reaction at pores bottom (R_2C_2) for the reference sample (left side) and the sample with chlorides (right side).

No chlorides				With chlorides		
Temp. (^{0}C)	R_2, (MΩ cm^2)	C_2 (μF/cm^2)	α_2	R_2 (MΩ cm^2)	C_2 (μF/ cm^2)	α_2
5	1.0	133.2	0.8	1.8	169.8	0.7
10	2.0	103.9	0.8	2.0	254.0	0.6
15	2.1	126.2	0.8	1.5	410.0	0.7
20	4.1	105.2	0.8	1.5	239.7	0.8
25	57.3	122.3	0.8	0.1	739.5	0.7
30	100.0	150.0	0.8	0.4	269.6	0.7
35	99.1	153.9	0.8	1.2	151.7	0.8
40	92.6	194.9	0.8	0.5	169.8	0.8
45	92.5	215.7	0.8			

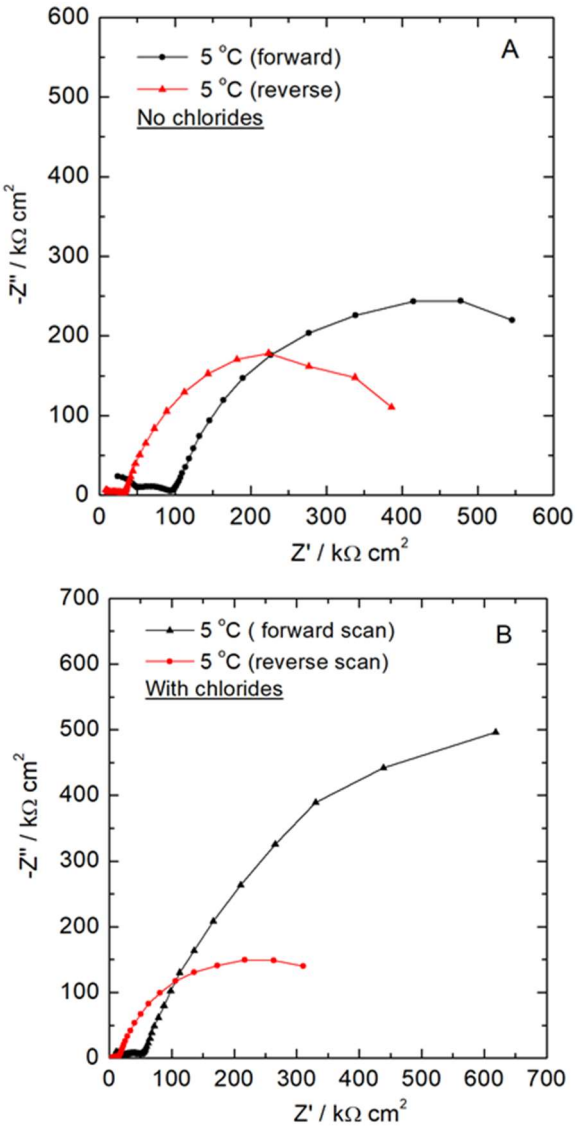

Fig. 7. Comparison of the EIS spectra at 5 ºC, at the initial stage and after the thermal cycle depicted in Fig. 2. Figures A) and B) compare the effect of the thermal cycle within the same mortar chemistry (without and with chlorides, respectively).

impedance becomes decreased by a similar proportion, due to the increased active surface at the pore's bottom.

Figure 7B shows that, in the presence of chlorides, the thermal cycle also generates new defects in the coating, but the decrease observed for the low frequency limit of the impedance is proportionally higher, which represents an additional accelerating effect to the corrosion process, probably the balance change of free chlorides.

Comparing Figs. 7A and 7B, it easy to see the difference in percolating pore density and/or electrolyte conductivity from the diameter of the high frequency arcs, which is double for the sample without chlorides. This fact is also evident from Fig. 8A.

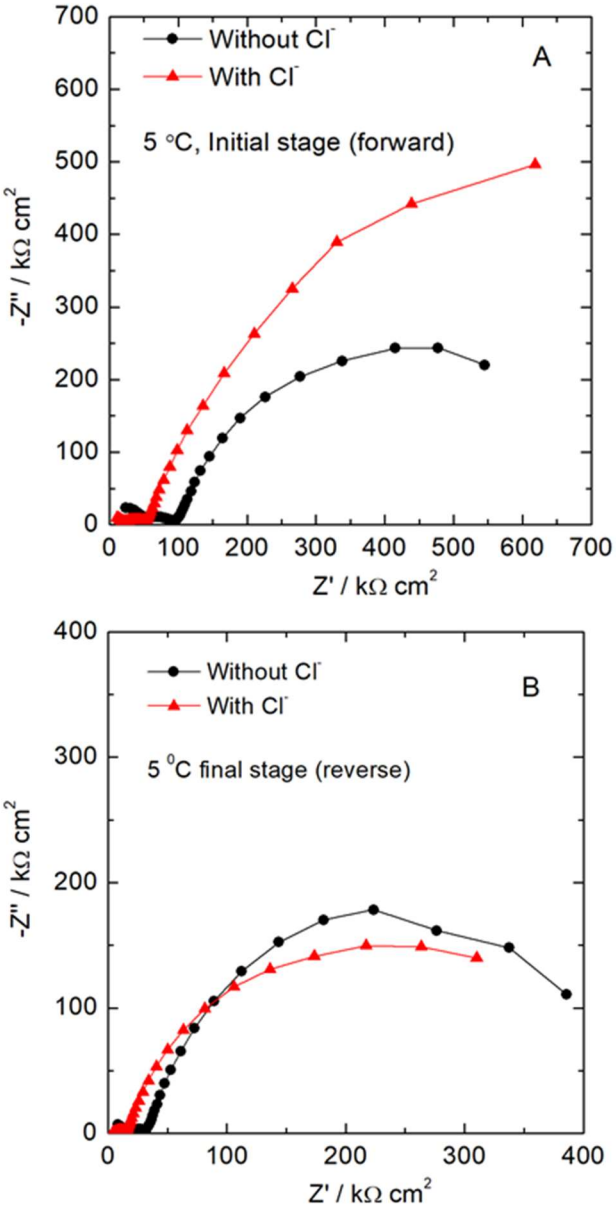

Fig. 8. Comparison of the EIS spectra at 5 ºC, at the initial stage and after the thermal cycle depicted in Fig. 2.Figures A) and B) compare the effect of the thermal cycle between distinct mortar chemistries (initial stage and final stage, respectively).

Figures 8A and 8B show the activating effect of chlorides when comparing the low frequency part of the spectra. At the initial stage (Fig. 8A), the diameter of the capacitive arc is higher for the sample containing chlorides. However, after the thermal cycle (Fig. 8B), both low frequency limits converge, which again informs about the activation effects beyond the Fe^{2+}/Fe^{3+} transformations typical for the system without chlorides.

4.0 CONCLUSIONS

From the above-discussed results, obtained on atmosphere-aged reinforced mortar samples, we conclude that:

a) EIS allows differentiating between the bulk mortar, the oxides layer, and the metal-solution interface contributions to the impedance of the system.
b) Temperature is a key parameter in the electrochemical behaviour of the system and affects the three regions discussed. Thermal cycles induce the formation of ionic paths in both the mortar cover and the oxides layer.
c) The contribution of the oxides layer to the impedance spectra was identified in the 10 kHz-1 Hz frequency range. The oxides layer supports the oxygen cathodic reaction, but also the anodic and cathodic processes corresponding to the re-oxidation and reduction of the layer itself.
d) Compared to layers formed in the absence of chlorides, the presence of chlorides in the concrete mix leads to the formation of more oxidised oxide layers, with decreased redox activity and more prone to crack formation under thermal cycling.

Acknowledgement

The authors acknowledge the local government Xunta the Galicia for financial support under grant ED431B2017/65-GPC.

References

Alonso, C, C Andrade, M Castellote, and P Castro. 2000. "Chloride Threshold Values to Depassivate Reinforcing Bars Embedded in a Standardized OPC Mortar." Cement and Concrete Research 30 (7): 1047–55. doi:10.1016/S0008-8846(00)00265-9.

Alonso, C, C Andrade, X. R. Nóvoa, M Izquierdo, and M. C. Pérez. 1998. "Effect of Protective Oxide Scales in the Macrogalvanic Behaviour of Concrete Reinforcements." Corrosion Science 40 (8): 1379–89. doi:10.1016/S0010-938X(98)00040-7.

Andrade, C., C. Alonso, and J Sarría. 2002. "Corrosion Rate Evolution in Concrete Structures Exposed to the Atmosphere." Cement and Concrete Composites 24 (1): 55–64. doi:10.1016/S0958-9465(01)00026-9.

Andrade, C, M Keddam, X. R. Nóvoa, M. C. Pérez, C. M. Rangel, and H Takenouti. 2001. “Electrochemical Behaviour of Steel Rebars in Concrete: Influence of Environmental Factors and Cement Chemistry.” Electrochimica Acta 46 (24–25): 3905–12. doi:10.1016/S0013-4686(01)00678-8.

Andrade, C, P Merino, X. R. Nóvoa, M. C. Pérez, and L Soler. 1995. “Passivation of Reinforcing Steel in Concrete.” Materials Science Forum 192–194 (pt 2): 891–98. doi:10.4028/www.scientific.net/MSF.192-194.891.

Andrade, C, L Soler, C Alonso, X R Nóvoa, and M Keddam. 1995. “The Importance of Geometrical Considerations in the Measurement of Steel Corrosion in Concrete by Means of AC Impedance.” Corrosion Science 37 (12): 2013–23. doi:10.1016/0010-938X(95)00095-2.

Bautista, A, E.C. Paredes, F Velasco, and S.M. Alvarez. 2015. “Corrugated Stainless Steels Embedded in Mortar for 9years: Corrosion Results of Non-Carbonated, Chloride-Contaminated Samples.” Construction and Building Materials 93 (September). Elsevier Ltd: 350–59. doi:10.1016/j.conbuildmat.2015.04.060.

Deus, J.M., L. Freire, M.F. Montemor, and X.R. Nóvoa. 2012. “The Corrosion Potential of Stainless Steel Rebars in Concrete: Temperature Effect.” Corrosion Science 65 (December): 556–60. doi:10.1016/j.corsci.2012.09.001.

Díaz, B., B. Guitián, X. R. Nóvoa, and M. C. Pérez. 2018. “The Effect of Long-Term Atmospheric Aging and Temperature in the Electrochemical Behaviour of Steel Rebars in Mortar.” Corrosion Science, submitted.

Díaz, B, L Freire, M Mojío, and X.R. Nóvoa. 2015. “Optimization of Conversion Coatings Based on Zinc Phosphate on High Strength Steels, with Enhanced Barrier Properties.” Journal of Electroanalytical Chemistry 737 (January): 174–83. doi:10.1016/j.jelechem.2014.06.035.

Flis, J. 1996. “Impedance Study of Reinforcing Steel in Simulated Pore Solution with Tannin.” Journal of The Electrochemical Society 143 (8): 2458–64. doi:10.1149/1.1837031.

Freire, L, M.A. Catarino, M.I. Godinho, M.J. Ferreira, M.G.S. Ferreira, A.M.P. Simões, and M.F. Montemor. 2012. “Electrochemical and Analytical Investigation of Passive Films Formed on Stainless Steels in Alkaline Media.” Cement and Concrete Composites 34 (9): 1075–81. doi:10.1016/j.cemconcomp.2012.06.002.

Ghods, P., O.B. Isgor, G. McRae, and T. Miller. 2009. “The Effect of Concrete Pore Solution Composition on the Quality of Passive Oxide Films on Black Steel Reinforcement.” Cement and Concrete Composites 31 (1). Elsevier Ltd: 2–11. doi:10.1016/j.cemconcomp.2008.10.003.

Guitián, B., S. Lascaud, X.R. Nóvoa, L. Ribeaucourt, and E. Vidal. 2013. “On the Growth of Nanostructured Iron Hydroxy-Fluorides for Li-Ion Batteries.” Journal of Power Sources 241 (November): 567–71. doi:10.1016/j.jpowsour.2013.04.145.

Joiret, S., M. Keddam, X. R. Nóvoa, M. C. Pérez, C. Rangel, and H. Takenouti. 2002. “Use of EIS, Ring-Disk Electrode, EQCM and Raman Spectroscopy to Study the Film of Oxides Formed on Iron in 1 M NaOH.” Cement and Concrete Composites 24 (1): 7–15. doi:10.1016/S0958-9465(01)00022-1.

Moreno, M., W. Morris, M.G. Alvarez, and G.S. Duffó. 2004. “Corrosion of Reinforcing Steel in Simulated Concrete Pore Solutions.” Corrosion Science 46 (11): 2681–99. doi:10.1016/j.corsci.2004.03.013.

Nóvoa, X.R., C. Pérez, A. Reyes, A. Soage, and A. Vázquez. 2016. “Thermogalvanic Currents in Steel Reinforced Concrete.” Electrochimica Acta 202 (June): 269–76. doi:10.1016/j.electacta.2015.11.138.

Park, J R, and D D Macdonald. 1983. “Impedance Studies of the Growth of Porous Magnetite Films on Carbon Steel in High Temperature Aqueous Systems.” Corrosion Science 23 (4): 295–315. doi:10.1016/0010-938X(83)90063-X.

Pour-Ghaz, M., O. Burkan Isgor, and P. Ghods. 2009. “The Effect of Temperature on the Corrosion of Steel in Concrete. Part 1: Simulated Polarization Resistance Tests and Model Development.” Corrosion Science 51 (2). Elsevier Ltd: 415–25. doi:10.1016/j.corsci.2008.10.034.

Sánchez-Moreno, M., H. Takenouti, J.J. García-Jareño, F. Vicente, and C. Alonso. 2009. “A Theoretical Approach of Impedance Spectroscopy during the Passivation of Steel in Alkaline Media.” Electrochimica Acta 54 (28): 7222–26. doi:10.1016/j.electacta.2009.07.013.

Sánchez, M., J. Gregori, C. Alonso, J.J. García-Jareño, H. Takenouti, and F. Vicente. 2007. “Electrochemical Impedance Spectroscopy for Studying Passive Layers on Steel Rebars Immersed in Alkaline Solutions Simulating Concrete Pores.” Electrochimica Acta 52 (27): 7634–41. doi:10.1016/j.electacta.2007.02.012.

Serdar, Marijana, Lidija Valek Žulj, and Dubravka Bjegović. 2013. “Long-Term Corrosion Behaviour of Stainless Reinforcing Steel in Mortar Exposed to Chloride Environment.” Corrosion Science 69: 149–57. doi:10.1016/j.corsci.2012.11.035.

Vidal, T., A. Castel, and R. François. 2007. “Corrosion Process and Structural Performance of a 17 Year Old Reinforced Concrete Beam Stored in Chloride Environment.” Cement and Concrete Research 37 (11): 1551–61. doi:10.1016/j.cemconres.2007.08.004.